

BiomedXPro: Prompt Optimization for Explainable Diagnosis with Biomedical Vision Language Models

Kaushitha Silva*
 University of Peradeniya
 Peradeniya, Sri Lanka
 e19372@eng.pdn.ac.lk

Ruwan Tennakoon
 RMIT University
 Melbourne, Australia
 ruwan.tennakoon@rmit.edu.au

Mansitha Eashwara*
 University of Peradeniya
 Peradeniya, Sri Lanka
 e19094@eng.pdn.ac.lk

Sanduni Ubayasiri*
 University of Peradeniya
 Peradeniya, Sri Lanka
 e19408@eng.pdn.ac.lk

Damayanthi Herath
 University of Peradeniya
 Peradeniya, Sri Lanka
 damayanthiherath@eng.pdn.ac.lk

Abstract

The clinical adoption of biomedical vision-language models is hindered by prompt optimization techniques that produce either uninterpretable latent vectors or single textual prompts. This lack of transparency and failure to capture the multi-faceted nature of clinical diagnosis, which relies on integrating diverse observations, limits their trustworthiness in high-stakes settings. To address this, we introduce BiomedXPro, an evolutionary framework that leverages a large language model as both a biomedical knowledge extractor and an adaptive optimizer to automatically generate a diverse ensemble of interpretable, natural-language prompt pairs for disease diagnosis. Experiments on multiple biomedical benchmarks show that BiomedXPro consistently outperforms state-of-the-art prompt-tuning methods, particularly in data-scarce few-shot settings. Furthermore, our analysis demonstrates a strong semantic alignment between the discovered prompts and statistically significant clinical features, grounding the model's performance in verifiable concepts. By producing a diverse ensemble of interpretable prompts, BiomedXPro provides a verifiable basis for model predictions, representing a critical step toward the development of more trustworthy and clinically-aligned AI systems.

1. Introduction

Accurate and transparent interpretation of biomedical images is fundamental for reliable disease diagnosis. In clinical practice, radiologists, pathologists, and other medical specialists rely on well-established visual cues such

as cellular morphology, tissue architecture, and pathological patterns, combined with domain expertise, to make informed diagnostic decisions. For computer vision systems to achieve clinical acceptance, they must not only demonstrate high predictive accuracy but also provide interpretable outputs that align with established clinical reasoning processes.

Recent advances in Vision-Language Models (VLMs), particularly Contrastive Language-Image Pre-training (CLIP) [14], have demonstrated remarkable potential for bridging visual content with natural language descriptions. Biomedical adaptations such as BiomedCLIP [21] extend these capabilities to medical imaging domains. While CLIP models demonstrate strong zero-shot capabilities, their performance often benefits from prompt optimization tailored to specific tasks. Early attempts relied on manual prompt engineering [14], which was labor-intensive and required domain expertise. To overcome these challenges, gradient-based prompt learning methods such as Context Optimization (CoOp) [24] introduced learnable soft prompts represented as continuous vectors optimized via gradient descent. Biomedical adaptations, including BiomedCoOp [10] and XCoOp [1], incorporated domain knowledge into CoOp frameworks to improve performance.

Despite these advances, two critical challenges remain for clinical adoption: (1) *prompts used to guide these models are typically optimized as uninterpretable feature vectors, providing no insight into the underlying diagnostic rationale* [1, 3, 10], and (2) *existing methods generally produce singular prompts, restricting their ability to capture the multifaceted nature of clinical observations that practitioners routinely consider*.

Large Language Models (LLMs) present a compelling

*Equal contribution

solution to these limitations. They can generate semantically meaningful, natural-language prompts that encode biomedical knowledge and can be automatically refined to enhance diagnostic performance [20, 25]. However, existing LLM-driven prompt optimization techniques still operate largely as black-box systems, with limited mechanisms to ensure clinical transparency or domain relevance.

In this work, we introduce *BiomedXPro*, an evolutionary prompting framework specifically designed for biomedical disease diagnosis. Unlike conventional methods that seek a single optimal prompt, our framework evolves a diverse ensemble of human-readable prompts, each capturing distinct diagnostic observations. These prompts may emphasize specific morphological alterations, tissue organizational patterns, or cellular-level abnormalities that are directly interpretable by clinical practitioners. We leverage LLMs both as biomedical knowledge extractors and as adaptive optimizers that iteratively refine prompts through structured feedback mechanisms, ensuring that the final prompt ensemble captures a comprehensive range of clinically meaningful features.

Our approach delivers three key advantages for clinical integration:

1. **Interpretability:** Each optimized prompt corresponds to a clear, medically grounded observation, providing transparency into model decision-making processes and enabling clinical validation.
2. **Diversity:** Maintaining multiple complementary prompts mirrors the multi-perspective approach that clinicians naturally employ when evaluating diagnostic evidence, enhancing model robustness and generalization capabilities.
3. **Clinical Trustworthiness:** Probabilistic predictions are anchored in semantically meaningful medical concepts, facilitating their integration into established diagnostic workflows and supporting evidence-based clinical decision-making.

By combining the adaptability of vision-language models with interpretable, LLM-driven prompt evolution, our framework goes beyond conventional accuracy-focused approaches and directly addresses the fundamental barriers to safe and trustworthy deployment of AI systems in clinical diagnostic environments.

2. Related work

2.1. VLMs in biomedical imaging

VLMs like CLIP [14] have revolutionized multi-modal learning by aligning images and text through contrastive pre-training, enabling strong zero-shot capabilities. However, their direct application to the biomedical domain is challenged by specialized terminology, subtle visual markers, and the scarcity of labeled data [22]. To overcome these

limitations, domain-adapted models such as MedCLIP [18], PubMedCLIP [4], and BiomedCLIP [21] have been developed. These models, by incorporating biomedical-specific pretraining strategies, have demonstrated superior performance on biomedical tasks.

BiomedCLIP, trained on over 15 million biomedical image-text pairs with a PubMedBERT encoder, has notably established state-of-the-art results across multiple biomedical vision-language benchmarks. While it offers strong zero-shot performance, its effectiveness can be further enhanced by adapting it to specific tasks. This is where prompt tuning becomes critical, as it efficiently tailors a frozen VLM for a new task without full model fine-tuning. This method involves optimizing a text prompt or its token level representation to guide the model toward the most relevant information, thereby capturing the fine-grained, disease-specific nuances that are essential in clinical applications and enhancing performance even in low-data settings.

2.2. Limitations of soft prompt tuning

Soft prompt tuning methods, which learn textual tokens appended to natural-language prompts, offer lightweight alternatives to full model fine-tuning. Context Optimization (CoOp) [24] introduced learnable soft prompts optimized via gradient descent under a frozen CLIP backbone. However, soft prompts often remain uninterpretable and may overfit in low-shot settings, limiting their applicability in high-stakes biomedical contexts where explainability is paramount. While recent adaptations like BiomedCoOp [10] and XCoOp [1] incorporate LLM-generated knowledge to improve performance and guide the learning process, they still fundamentally rely on uninterpretable soft prompts. Despite their advancements, the final learned prompts in these methods lack the true human-readability necessary for transparent and trustworthy clinical applications.

2.3. Hard prompt tuning

While soft prompts offer efficiency, their lack of transparency limits their use in clinical settings. Hard prompt tuning, which optimizes explicit text strings, improves interpretability but relies heavily on manual design and domain expertise. To overcome this, recent methods leverage LLMs for automated prompt generation. Approaches such as APE [25] and OPRO [20] treat prompt design as a black-box optimization problem, while frameworks like EvoPrompt [7] and PromptBreeder [5] integrate evolutionary algorithms to iteratively refine prompts, achieving stronger generalization than manual engineering.

These techniques have been extended to VLMs, with works such as Liu et al. [11] and IPO [3] demonstrating that interpretable, LLM-generated prompts reduce overfitting and improve transferability compared to gradient-based

CoOp. Evolutionary approaches like ProAPO [13] further improve efficiency by refining prompts through mutation and crossover while limiting repeated LLM queries.

Despite their promise, direct adaptation to biomedical imaging remains challenging. Many methods assume access to large general-domain corpora or rely on multimodal LLMs that struggle with biomedical specificity. Moreover, constraints such as limited initial prompt diversity (e.g., ProAPO) and incomplete integration of insights from broader prompt optimization research (e.g., handling recency bias, scoring formats) highlight open opportunities for advancing interpretable prompt tuning in BiomedCLIP and related models.

2.4. Explainability in biomedical CLIP models

Interpretability remains critical for clinical adoption. Extensions such as XCoOp [1] and BiomedCoOp [10] improve transparency by incorporating clinical knowledge extracted via LLMs, yet the learned soft prompts remain latent vectors with limited human readability.

An alternative is descriptor-based prompting, as in Xplainer [12], which classifies images based on structured radiological observations (e.g., “There is/are [no] [observation] indicating [pathology]”). This offers inherent interpretability, but its effectiveness depends on initial LLM-generated prompts and extensive manual engineering by domain experts, making it difficult to generalize across diverse biomedical tasks.

3. Methodology

3.1. Problem formulation

Given a biomedical dataset $\mathcal{D} = \{(x_i, y_i)\}_{i=1}^N$ with medical images $x_i \in \mathbb{R}^{H \times W \times C}$ and binary labels $y_i \in \{0, 1\}$, we address the challenge of learning interpretable visual concepts for disease classification. We leverage a pre-trained VLM with an image encoder $f_\theta : \mathbb{R}^{H \times W \times C} \rightarrow \mathbb{R}^d$ and a text encoder $g_\phi : \mathcal{T} \rightarrow \mathbb{R}^d$, which project visual and textual inputs into a shared d -dimensional embedding space.

Our goal is to discover a set of K semantically meaningful prompt pairs:

$$P = \{(p_j^-, p_j^+)\}_{j=1}^K, \quad p_j^-, p_j^+ \in \mathcal{T}, \quad (1)$$

where p_j^+ describes the presence of disease-indicative visual observations and p_j^- describes their absence or normal appearance.

Classification via prompt pairs. For each prompt pair (p_j^-, p_j^+) , we define a binary classifier based on cosine similarity in the shared embedding space:

$$h_j(x) = \mathbb{I}[\text{sim}(f_\theta(x), p_j^+) > \text{sim}(f_\theta(x), p_j^-)], \quad (2)$$

where $\text{sim}(x, p)$ denotes the ℓ_2 -normalized cosine similarity.

3.2. Evolutionary prompt optimization

We formulate prompt discovery as a multi-objective optimization problem that balances classification accuracy, which measures the collective performance of h_j on the training set, with prompt diversity, which mitigates semantic redundancy by penalizing similar prompts in the text embedding space. To address this problem, we propose an evolutionary algorithm that operates directly within the VLM embedding space and uses LLMs to generate semantically grounded prompt mutations. An overview of the proposed framework is shown in Figure 1, and the components of the algorithm are described below.

Initialization. We begin with a meta-prompt Q_0 that encodes key diagnostic observations, which is used to initialize the first-generation population:

$$P^{(0)} = \{(p_j^-, p_j^+)\}_{j=1}^{K_0}, \quad p_j^\pm \in \mathcal{T}, \quad (3)$$

where p_j^+ specifies a disease-related observation and p_j^- denotes its absence. The meta-prompt Q_0 template is as follows:

```
Give <K0> distinct textual
descriptions of pairs of visual
discriminative features to identify
<task description>. Only provide
the output as Python code in
the following format: prompts =
list[tuple[negative: str, positive:
str]].
```

Here, $<K_0>$ is the desired population size and $<\text{task description}>$ is instantiated for each task (e.g., “melanoma in dermoscopy images”)

Fitness evaluation & population update. Each prompt pair (p_j^-, p_j^+) is evaluated on the training set:

$$s_j = \mathcal{M}\left(\{h_j(x_i, y_i)\}_{x_i, y_i \in \mathcal{D}}\right). \quad (4)$$

where $\mathcal{M} : \{0, 1\}^N \times \{0, 1\}^N \rightarrow \mathbb{R}$ is a performance metric (e.g., accuracy, F1, or inverse binary cross-entropy).

Prompt pairs with $s_j \geq \alpha$ are retained in a memory buffer

$$\mathcal{U}^{(t)} = \{(p_j^-, p_j^+, s_j) \mid s_j \geq \alpha\}, \quad (5)$$

which aggregates high-performing prompts across generations. In practice $\mathcal{U}^{(t)}$ is capped to maintain tractable diversity.

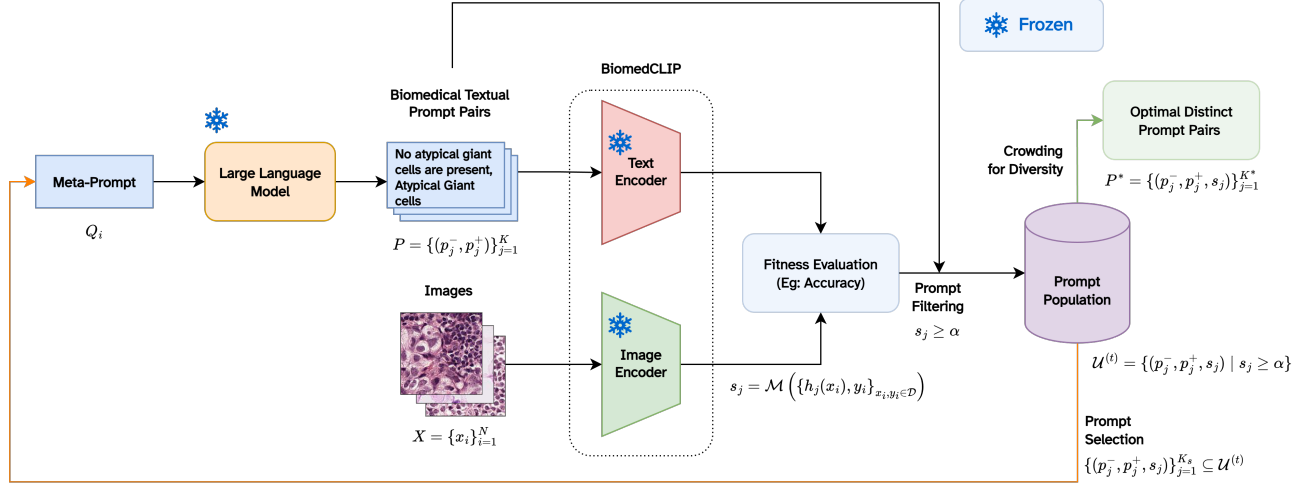


Figure 1. An overview of the BiomedXPro evolutionary framework. At each iteration, a LLM generates new prompt pairs (P) guided by a meta-prompt (Q_t) containing a subset of previously successful candidates. The prompts are evaluated using BiomedCLIP to compute a fitness score (s_j). High-performing prompts are filtered to populate a buffer ($\mathcal{U}^{(t)}$) from which the next generation’s candidates are selected. Finally, a crowding step is applied to the evolved population to yield a diverse, optimal set of prompts (P^*) for explainable diagnosis.

LLM-guided mutation. Unlike traditional evolutionary operators, we employ an LLM to generate refined prompt variations. Given selected prompts and their performance feedback, the LLM is instructed, via meta-prompt Q_t , to create K_t new prompt pairs that: (1) capture distinct medical concepts, (2) yield better performance.

At each iteration, a subset of K_s prompt pairs is drawn from the memory buffer $\mathcal{U}^{(t)}$ for mutation using roulette wheel selection [6] guided by fitness scores. This probabilistic strategy balances exploration of diverse prompts with a bias toward those of higher fitness. The structure of Q_t is shown below:

```

The task is to generate distinct
textual descriptions pairs <task
description>. Here are the best
performing pairs in ascending order.
High scores indicate higher quality.
Current Top <K_s> prompt pairs:
<List of prompt pairs with
normalized scores>
Write <K_t> new prompt pairs that
are different from the old ones and
have a score as high as possible.
Formulate a strategy. Only provide
the output as Python code...Let's
think step-by-step
  
```

The meta-prompt’s design is critical for effective generation. While sampled via roulette wheel for diversity, the in-context examples are framed as the “top performing pairs”

to provide a clear optimization signal. To counteract recency bias [20], these exemplars are sorted in ascending order of fitness. Based on findings from Yang *et al.* [20], scores are normalized to an integer range [60-90] for stability. Finally, Chain-of-Thought prompting [19] is enabled via “Formulate a strategy” and “Let’s think step-by-step” to elicit reasoned generation.

Crowding for Diversity. After all T generations have completed, we apply a crowding mechanism inspired by NSGA-II [2] to the final candidate pool $\mathcal{U}^{(T)}$ to eliminate semantic redundancy. Candidate prompts are clustered by semantic similarity via an LLM guided by the meta-prompt Q^{crowd} :

```

The task is to group textual
description pairs...
<Numbered List of K_c prompt pairs>
Group the prompt pairs that has
exactly same observation but differ
only in language variations. Give
the indexes of the grouped pairs
in the output. Provide the output
as follows: list[list[index:int]].
Make sure to include all pairs in
the output, even if they are not
grouped with others. Let's think
step by step
  
```

This prompt instructs the LLM to act as a semantic de-duplicator, grouping prompts that describe the same core

Algorithm 1: Evolutionary Prompt Optimization for Biomedical Classification

Input: Dataset $\mathcal{D} = \{(x_i, y_i)\}_{i=1}^N$, pre-trained encoders f_θ, g_ϕ , meta-prompts $\{Q_0, Q_t, Q_t^{\text{crowd}}\}$, threshold α , generations T , initial population size K_0 , sampling size K_s , generation size K_t .
Output: Optimized prompt set P^* .
Initialization: Generate initial population $P^{(0)}$ by prompting LLM with Q_0 .
for $t = 1$ **to** T **do**
 foreach (p_j^-, p_j^+) **in** $P^{(t-1)}$ **do**
 Evaluate fitness s_j using performance metric \mathcal{M} ;
 Update memory buffer $\mathcal{U}^{(t)}$ with prompts satisfying $s_j \geq \alpha$;
 Selection: Sample K_s prompt pairs from $\mathcal{U}^{(t)}$ using roulette-wheel selection guided by s_j ;
 Mutation: Use LLM with meta-prompt Q_t to generate new prompt pairs $P^{(t)}$ emphasizing diversity and higher performance;
Final Crowding: Remove redundant prompts from $\mathcal{U}^{(T)}$ to obtain P^* ;
Prediction: Aggregate classifiers using weighted majority voting.

observation despite linguistic differences. Within each cluster returned by the LLM, only the highest-scoring pair is retained. The resulting set of unique, high-performing prompts constitutes our final optimized prompt set, P^* :

$$P^* \leftarrow \bigcup_{c \in \mathcal{C}} \underset{(p^-, p^+, s) \in c}{\operatorname{argmax}} s. \quad (6)$$

Final Prediction. For the final prediction, the optimized set of prompts $P^* \subseteq \mathcal{U}^{(T)}$ is aggregated via weighted majority voting:

$$\hat{y} = \mathbb{I} \left[\sum_{j=1}^{K^*} w_j h_j(x) > \frac{1}{2} \sum_{j=1}^{K^*} w_j \right], \quad (7)$$

where each weight w_j is set to the corresponding fitness score s_j over validation data, ensuring that more reliable prompts contribute more strongly to the final decision.

The complete BiomedXPro framework is summarized in Algorithm 1.

4. Experiments and results

4.1. Experimental setup

We evaluate our proposed BiomedXPro framework on a diverse set of biomedical tasks, with a specific focus on its ability to generate interpretable and high-performing prompts for few-shot learning and generalization. All experiments were conducted using the same base models for a fair comparison and were run on a single NVIDIA GeForce RTX 3090 Ti GPU.

Base models. For the VLM, we employed BiomedCLIP [10] with a ViT-B/16 backbone, a model that has demonstrated state-of-the-art zero-shot classification on various biomedical benchmarks. For the LLM, we employed Gemma 3-27B-it [16], accessed via Google AI Studio with default model parameters (temperature, top-k, top-p).

Datasets. We evaluate on three public benchmarks spanning diverse imaging modalities: Derm7pt [8] (dermoscopy), WBCAtt [17] (peripheral blood smears), and Camelyon17-WILDS [9] (histopathology). Camelyon17-WILDS enables domain generalization assessment, with hospitals serving as distinct domains, while Derm7pt and WBCAtt are used to evaluate interpretability and clinical relevance. Meta-prompts used for each dataset is provided in the supplementary material.

Experimental protocols and evaluation. We consider three evaluation protocols. (i) Few-shot learning: varying the number of labeled samples per class ($N_c \in 1, 2, 4, 8, 16$) to assess data efficiency. (ii) Clinical relevance: assessing whether high-fitness prompts capture clinically validated concepts, using Derm7pt and WBCAtt. For Derm7pt, we restrict to binary melanoma versus non-melanoma classification, while WBCAtt is extended to a multiclass setting via one-vs-rest binary classifiers. (iii) Domain generalization: training on three hospital domains of Camelyon17-WILDS and evaluating on the unseen hospital domain.

We compare against zero-shot BiomedCLIP and representative prompt-tuning approaches, including CoOp [24], CoCoOp [23], and their biomedical extensions BiomedCoOp [10] and XCoOp [1]. For all prompt-tuning baselines, we adopt the default hyperparameters (e.g., learning rate, training epochs, number of LLM prompts) from the official BiomedCoOp implementation to ensure a fair comparison. Given the class imbalance inherent in biomedical datasets, we use the F1-macro score as our primary evaluation metric. Given the class imbalance inherent in biomedical datasets, we use the **F1-macro** score as our primary evaluation metric.

BiomedXPro parameters. The evolutionary search is run for 500 generations ($T = 500$), initialized with a population of 50 prompt pairs ($K_0 = 50$). In each generation, we sample 10 candidates ($K_s = 10$) for mutation and instruct the LLM to generate 10 new refinements ($K_t = 10$), while maintaining a memory buffer of up to 1000 pairs to preserve diversity. Fitness is evaluated using the inverse binary cross-entropy for the 1- and 2-shot settings, and the F1-macro score for higher-shot regimes. The fitness threshold α is set relative to the zero-shot baseline, ensuring that prompts performing below chance for the chosen metric are discarded. Final crowding is performed over 3 iterations on batches of 30 pairs. Results are averaged over three independent runs.

4.2. Results and analysis

Quantitative performance. BiomedXPro consistently outperforms all baselines in the data-scarce few-shot regime (Table 1). Its advantage is most pronounced in the critical 1–8 shot range, demonstrating strong generalization across the diverse tasks and imaging modalities represented by the benchmarks.

A notable trend is the underperformance of BiomedCoOp, and XCoOp compared to standard CoOp and CoCoOp. We hypothesize that this stems from its reliance on a single static LLM-generated prompt to inject biomedical knowledge. In our optimization framework, we observed that single-query LLM prompts often yield suboptimal solutions, effectively constraining the search space and leading to weaker generalization. By contrast, BiomedXPro continually explores and refines prompt candidates, avoiding this limitation and converging toward a diverse ensemble of high-fitness solutions

Full-data regime. To assess whether our method remains competitive in data-abundant settings, we evaluate on the full Derm7pt dataset. Results are shown in Table 2. BiomedXPro remains comparable to the strongest baseline (XCoOp), while offering the added advantage of interpretable prompts. This indicates that our framework does not sacrifice performance even when abundant labeled data is available.

Clinical relevance. To validate that BiomedXPro learns clinically relevant concepts, we analyze the semantic alignment between the discovered prompts and the training data’s statistical features. Specifically, we compute the conditional probability $P(\text{class} \mid \text{observation})$ across the training dataset to ground our analysis. The full conditional probabilities are provided in the supplementary material. The following analysis demonstrates a strong correspondence between these statistics and the semantic content of the discovered prompts.

For the **Derm7pt** task, the analysis reveals a strong correlation. The most statistically significant indicator, **‘Linear Irregular’ vascular structures** ($P = 0.80$), was captured by a high-fitness prompt pair (F1: 0.6523) contrasting a *‘regular, linear arrangement’* with a *‘chaotic, branching pattern.’* Other key features like the **‘Blue-Whitish Veil’** ($P = 0.59$) were also identified by high-scoring prompts (F1: 0.6667) that distinguished its absence from when it is *‘present and associated with ulceration.’* Furthermore, the prompts with the highest F1-scores (up to 0.6741) corresponded to another strong indicator, **‘Atypical Pigment Network’** ($P = 0.55$), by providing nuanced descriptions such as *‘variegated pigmentation with shades of brown, black, blue, and grey.’*

Similarly, For **Neutrophil** classification on WBCAtt, the framework again captured the most predictive features. For instance, the presence of **small granules** ($P = 1.00$) was identified by a prompt contrasting *‘clear and homogenous’* cytoplasm with cytoplasm that *“contains fine, pale lilac granules,”* while the highly predictive **unsegmented-band nucleus** ($P = 0.85$) was described by a prompt distinguishing a *‘predominantly spherical’* nucleus from one that is *“irregular and lobulated.”* This consistent alignment across tasks demonstrates that the framework’s evolutionary process discovers and textually articulates statistically significant visual features in an interpretable manner. The complete prompt ensembles (P^*) discovered for both Derm7pt and WBCAtt are provided in the supplementary material.

4.3. Ablation studies

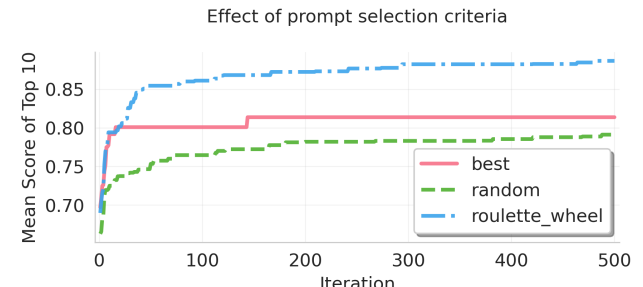


Figure 2. Effect of prompt selection strategy on convergence. Our proposed *Roulette Wheel* selection achieves the best balance of exploration and exploitation, leading to more stable and consistent performance gains compared to *Best-N* and *Random* selection.

Effect of prompt selection criteria. We analyze the impact of the strategy for sampling mutation candidates by comparing our proposed *Roulette Wheel Selection* against two baselines: deterministic *Best-N* and uniform *Random* selection. As shown in Fig. 2, these baselines represent extremes of the exploration-exploitation trade-off. *Best-N* selection focuses purely on exploitation, leading to premature

Table 1. F1-macro percentage results of BiomedXPro compared with baseline methods across zero-shot and few-shot settings. Camelyon17-WILDS is evaluated in a domain generalization setup (train on 3 hospitals, test on unseen). Derm7pt is restricted to binary melanoma vs. non-melanoma. WBCAtt is extended to multiclass classification via one-vs-rest classifiers.

Dataset	Method	1-Shot	2-Shot	4-Shot	8-Shot	16-Shot
Camelyon17WILDS	Zero-shot			41.93		
	CoOp	78.79	70.76	74.15	84.25	88.47
	CoCoOp	76.43	66.13	75.19	85.13	86.88
	BiomedCoOp	53.15	61.06	58.69	63.46	56.94
	XCoOp	66.90	35.60	45.00	64.20	84.50
BiomedXPro(Ours)		72.06	86.95	90.20	90.87	90.38
Derm7pt	Zero-shot			27.86		
	CoOp	33.91	55.88	58.70	54.92	61.38
	CoCoOp	33.89	56.70	50.97	54.36	57.06
	BiomedCoOp	52.49	57.22	45.96	51.30	61.46
	XCoOp	39.50	58.70	60.10	41.90	54.80
BiomedXPro(Ours)		64.54	61.45	60.87	58.51	64.17
WBCAtt	Zero-shot			10.50		
	CoOp	33.08	41.74	55.10	67.81	75.5
	CoCoOp	31.86	41.91	55.96	62.02	72.19
	BiomedCoOp	11.24	10.83	10.48	10.57	10.91
	XCoOp	26.20	22.10	22.80	25.20	28.9
BiomedXPro(Ours)		41.39	47.31	58.33	69.63	72.18

Table 2. Full-data Derm7pt results (F1-macro).

Method	F1-macro
BiomedXPro (Ours)	71.14
BiomedCoOp	59.02
CoOp	67.91
XCoOp	75.60
CoCoOp	67.68

convergence in local optima, while *Random* selection’s pure exploration provides an inefficient and erratic search signal to the LLM. Our approach effectively balances this trade-off by probabilistically favoring higher-fitness candidates while maintaining sufficient randomness for exploration, resulting in the stable and consistent performance gains shown in the learning curves.

Impact of generation size per iteration. We also analyze the number of prompt pairs generated per mutation step, comparing our choice of 10 against smaller (5) and larger (50) sets. As shown in Fig. 3, generating only 5 pairs leads to slow convergence, while a large set of 50 causes performance to plateau quickly after a strong start. While the precise reason for this degradation with a large generation size is unclear, this finding is consistent with prior work by Yang *et al.* [20], who also observed that a moderate number of generated instructions was optimal. Based on these findings, we utilize a generation size of 10, as it provides

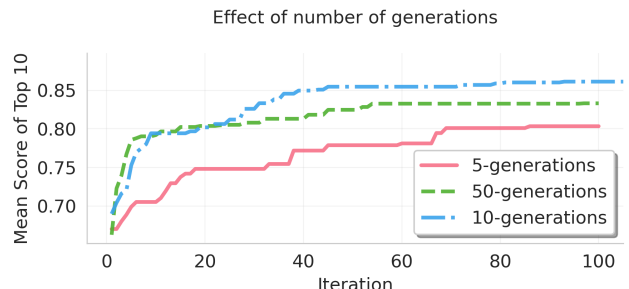


Figure 3. Impact of generation size per iteration on performance. The 10-pair setting (our choice) provides the optimal balance, outperforming 5 pairs and 50 pairs.

a favorable balance between refinement diversity and optimization stability while being more cost-effective in terms of token usage.

Effect of chain-of-thought prompting. We investigated the effect of Chain-of-Thought (CoT) prompting by adding an instruction for the LLM to first “formulate a strategy” and “Let’s think step-by-step” for improvement before generating new candidates. As shown in Fig. 4, this addition leads to consistently better performance. Examples of CoT generated by the LLM are provided in the supplementary material.

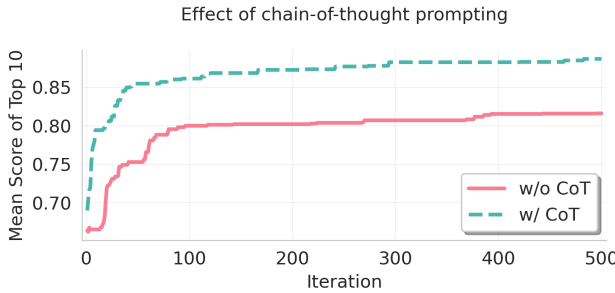


Figure 4. Effect of Chain-of-Thought (CoT) prompting, which consistently outperforms a direct-instruction baseline.

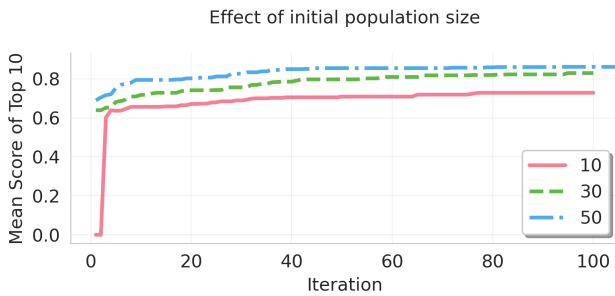


Figure 5. Effect of initial population size on performance. A larger and more diverse initial population (50) consistently outperforms smaller sets

Effect of initial population size. We compare initial sizes K_0 of 10, 30, and 50, and find that a larger initial population of 50 consistently outperforms the smaller sets (Fig. 5). This suggests that a broader initial semantic space provides a more robust foundation for the optimization, preventing premature convergence on a narrow range of concepts. We did not explore sizes beyond 50 due to the practical limitations of our LLM, which struggled to reliably generate a large and exact number of distinct prompts in a single query.

4.4. Limitations and future work

Dependencies on pre-trained models and data. The efficacy of BiomedXPro is fundamentally dependent on two core components: the underlying LLM and VLM. The framework’s ability to generate clinically relevant prompts is inherently capped by the breadth and accuracy of the biomedical knowledge encoded within the LLM, creating a potential knowledge bottleneck. While state-of-the-art commercial models like GPT-4 (used by XCoOp [1] and BiomedCoOp [10]) contain extensive knowledge, their use in an iterative framework with hundreds of generations is prohibitively expensive, necessitating a trade-off between model capability and computational cost. Similarly, the framework’s performance is tied to the VLM’s ability to form a meaningful embedding space, and it may inherit bi-

ases from the VLM’s pre-training data, potentially affecting fairness across diverse patient populations, an important area for further investigation.

Architectural limitations and validation assumptions. Architecturally, the proposed framework is formulated for binary classification. While effective in multiclass settings via a one-vs-rest scheme, this approach can lead to over-specialized negative prompts (p_j^-) that describe a single competing class (e.g., contrasting ‘Eosinophils’ with ‘Neutrophils’) rather than a general negative case. Extending the framework to natively handle multiclass prompt sets (instead of a prompt pair) is a non-trivial future research direction that must address the combinatorial complexity of updating the prompt set. Another architectural limitation is that diversity is enforced via crowding only as a final post-processing step. We found that per-iteration LLM-driven clustering was unstable, sometimes erroneously grouping disparate prompts. Future work could integrate diversity maintenance at each optimization step by using a more deterministic semantic similarity metric on the prompts or the prompt embeddings. Furthermore, our validation approach in this work relies on training data statistics as a proxy for clinical importance, a measure that may itself be subject to dataset-specific biases.

Future work in clinical verification and grounding. Finally, building full clinical trust requires deeper verification of the model’s reasoning. While our framework generates highly descriptive prompts (e.g., ‘variegated pigmentation with shades of brown, black, blue, and grey’), future work is needed to verify that the VLM’s decision-making is truly sensitive to such nuanced details. A comprehensive validation would also require visual grounding analysis, using methods like Grad-CAM [15], to ensure the model’s spatial attention aligns with the features described in the prompts. Both steps, coupled with rigorous evaluation by clinical domain experts, are essential for ensuring the model’s reasoning process is robust and truly aligned with clinical practice.

5. Conclusion

In this work, we introduce BiomedXPro, an evolutionary framework that generates diverse ensembles of interpretable, natural-language prompts for biomedical image classification. Our method addresses the critical limitations of uninterpretable soft prompts and single-prompt systems by leveraging an LLM as both a biomedical knowledge extractor and an adaptive optimizer within an evolutionary search.

Our experiments demonstrate that BiomedXPro consistently outperforms state-of-the-art prompt-tuning methods

in challenging few-shot and domain generalization settings across multiple biomedical datasets. Crucially, our analysis shows that the discovered prompts are not only high-performing but are also semantically aligned with statistically significant clinical features, grounding the model’s predictions in verifiable concepts. By directly addressing the fundamental needs for interpretability, diversity, and trustworthiness, BiomedXPro represents a significant step toward the safe and reliable deployment of advanced vision-language models in clinical practice.

References

[1] Yequan Bie, Luyang Luo, Zhixuan Chen, and Hao Chen. Xcoop: Explainable prompt learning for computer-aided diagnosis via concept-guided context optimization. In *International Conference on Medical Image Computing and Computer-Assisted Intervention*, pages 773–783. Springer, 2024. [1](#), [2](#), [3](#), [5](#), [8](#)

[2] Kalyanmoy Deb, Amrit Pratap, Sameer Agarwal, and T. Meiyarivan. A fast and elitist multiobjective genetic algorithm: Nsga-ii. *IEEE Transactions on Evolutionary Computation*, 6(2):182–197, 2002. [4](#)

[3] Yingjun Du, Wenfang Sun, and Cees G M Snoek. IPO: Interpretable Prompt Optimization for Vision-Language Models. [1](#), [2](#)

[4] Sedigheh Eslami, Christoph Meinel, and Gerard de Melo. PubMedCLIP: How Much Does CLIP Benefit Visual Question Answering in the Medical Domain? In *Findings of the Association for Computational Linguistics: EACL 2023*, pages 1181–1193, Dubrovnik, Croatia, 2023. Association for Computational Linguistics. [2](#)

[5] Chrisantha Fernando, Dylan Banarse, Henryk Michalewski, Simon Osindero, and Tim Rocktäschel. Promptbreeder: Self-Referential Self-Improvement Via Prompt Evolution, 2023. arXiv:2309.16797 [cs]. [2](#)

[6] David E. Goldberg. Genetic algorithms in search, optimization, and machine learning. In *Addison-Wesley Longman Publishing Co., Inc.* 1989. [4](#)

[7] Qingyan Guo, Rui Wang, Junliang Guo, Bei Li, Kaitao Song, Xu Tan, Guoqing Liu, Jiang Bian, and Yujiu Yang. Evo-Prompt: Connecting LLMs with Evolutionary Algorithms Yields Powerful Prompt Optimizers, 2025. arXiv:2309.08532 [cs]. [2](#)

[8] Jeremy Kawahara, Sara Daneshvar, Giuseppe Argenziano, and Ghassan Hamarneh. Seven-Point Checklist and Skin Lesion Classification Using Multitask Multimodal Neural Nets. *IEEE Journal of Biomedical and Health Informatics*, 23(2):538–546, 2019. [5](#)

[9] Pang Wei Koh, Shiori Sagawa, Henrik Marklund, Sang Michael Xie, Marvin Zhang, Akshay Balsubramani, Weihua Hu, Michihiro Yasunaga, Richard Lanas Phillips, Irena Gao, Tony Lee, Etienne David, Ian Stavness, Wei Guo, Berton A. Earnshaw, Imran S. Haque, Sara Beery, Jure Leskovec, Anshul Kundaje, Emma Pierson, Sergey Levine, Chelsea Finn, and Percy Liang. WILDS: A Benchmark of in-the-Wild Distribution Shifts, 2021. arXiv:2012.07421 [cs]. [5](#)

[10] Taha Koleilat, Hojat Asgariandehkordi, Hassan Rivaz, and Yiming Xiao. BiomedCoOp: Learning to Prompt for Biomedical Vision-Language Models, 2025. arXiv:2411.15232 [cs]. [1](#), [2](#), [3](#), [5](#), [8](#)

[11] Shihong Liu, Samuel Yu, Zhiqiu Lin, Deepak Pathak, and Deva Ramanan. Language Models as Black-Box Optimizers for Vision-Language Models. In *2024 IEEE/CVF Conference on Computer Vision and Pattern Recognition (CVPR)*, pages 12687–12697, Seattle, WA, USA, 2024. IEEE. [2](#)

[12] Chantal Pellegrini, Matthias Keicher, Ege Özsoy, Petra Jiraskova, Rickmer Braren, and Nassir Navab. Xplainer: From X-Ray Observations to Explainable Zero-Shot Diagnosis, 2023. arXiv:2303.13391 [cs]. [3](#)

[13] Xiangyan Qu, Gaopeng Gou, Jiamin Zhuang, Jing Yu, Kun Song, Qihao Wang, Yili Li, and Gang Xiong. ProAPO: Progressively Automatic Prompt Optimization for Visual Classification, 2025. arXiv:2502.19844 [cs]. [3](#)

[14] Alec Radford, Jong Wook Kim, Chris Hallacy, Aditya Ramesh, Gabriel Goh, Sandhini Agarwal, Girish Sastry, Amanda Askell, Pamela Mishkin, Jack Clark, Gretchen Krueger, and Ilya Sutskever. Learning Transferable Visual Models From Natural Language Supervision, 2021. arXiv:2103.00020 [cs]. [1](#), [2](#)

[15] Ramprasaath R. Selvaraju, Michael Cogswell, Abhishek Das, Ramakrishna Vedantam, Devi Parikh, and Dhruv Batra. Grad-CAM: Visual Explanations from Deep Networks via Gradient-based Localization. *International Journal of Computer Vision*, 128(2):336–359, 2020. arXiv:1610.02391 [cs]. [8](#)

[16] Gemma Team, Aishwarya Kamath, Johan Ferret, Shreya Pathak, Nino Vieillard, Ramona Merhej, Sarah Perrin, Tatiana Matejovicova, Alexandre Ramé, Morgane Rivière, Louis Rouillard, Thomas Mesnard, Geoffrey Cideron, Jean bastien Grill, Sabela Ramos, Edouard Yvinec, Michelle Casbon, Etienne Pot, Ivo Penchev, Gaël Liu, Francesco Visin, Kathleen Kenealy, Lucas Beyer, Xiaohai Zhai, Anton Tsitsulin, Robert Busa-Fekete, Alex Feng, Noveen Sachdeva, Benjamin Coleman, Yi Gao, Basil Mustafa, Iain Barr, Emilio Parisotto, David Tian, Matan Eyal, Colin Cherry, Jan-Thorsten Peter, Danila Sinopalnikov, Surya Bhupatiraju, Rishabh Agarwal, Mehran Kazemi, Dan Malkin, Ravin Kumar, David Vilar, Idan Brusilovsky, Jiaming Luo, Andreas Steiner, Abe Friesen, Abhanshu Sharma, Abheesht Sharma, Adi Mayrav Gilady, Adrian Goedeckemeyer, Alaa Saade, Alex Feng, Alexander Kolesnikov, Alexei Bendebury, Alvin Abdagic, Amit Vadi, András György, André Susano Pinto, Anil Das, Ankur Bapna, Antoine Miech, Antoine Yang, Antonia Patterson, Ashish Shenoy, Ayan Chakrabarti, Bilal Piot, Bo Wu, Bobak Shahriari, Bryce Pettrini, Charlie Chen, Charline Le Lan, Christopher A. Choquette-Choo, CJ Carey, Cormac Brick, Daniel Deutscher, Danielle Eisenbud, Dee Cattie, Derek Cheng, Dimitris Paparas, Divyashree Shivakumar Sreepathihalli, Doug Reid, Dustin Tran, Dustin Zelle, Eric Noland, Erwin Huizenga, Eugene Kharitonov, Frederick Liu, Gagik Amirkhanyan, Glenn Cameron, Hadi Hashemi, Hanna Klimczak-Plucińska, Harman Singh, Harsh Mehta,

Harshal Tushar Lehri, Hussein Hazimeh, Ian Ballantyne, Idan Szpektor, Ivan Nardini, Jean Pouget-Abadie, Jetha Chan, Joe Stanton, John Wieting, Jonathan Lai, Jordi Orbay, Joseph Fernandez, Josh Newlan, Ju yeong Ji, Jyotinder Singh, Kat Black, Kathy Yu, Kevin Hui, Kiran Vodrahalli, Klaus Greff, Linhai Qiu, Marcella Valentine, Marina Coelho, Marvin Ritter, Matt Hoffman, Matthew Watson, Mayank Chaturvedi, Michael Moynihan, Min Ma, Nabila Babar, Natasha Noy, Nathan Byrd, Nick Roy, Nikola Momichev, Nilay Chauhan, Noveen Sachdeva, Oskar Bunyan, Pankil Botarda, Paul Caron, Paul Kishan Rubenstein, Phil Culliton, Philipp Schmid, Pier Giuseppe Sessa, Pingmei Xu, Piotr Stanczyk, Pouya Tafti, Rakesh Shivanna, Renjie Wu, Renke Pan, Reza Rokni, Rob Willoughby, Rohith Vallu, Ryan Mullins, Sammy Jerome, Sara Smoot, Sertan Girgin, Shariq Iqbal, Shashir Reddy, Shruti Sheth, Siim Põder, Sijal Bhattacharya, Sindhu Raghuram Panyam, Sivan Eiger, Susan Zhang, Tianqi Liu, Trevor Yacovone, Tyler Liechty, Uday Kalra, Utku Evcı, Vedant Misra, Vincent Roseberry, Vlad Feinberg, Vlad Kolesnikov, Woohyun Han, Woosuk Kwon, Xi Chen, Yinlam Chow, Yuvein Zhu, Zichuan Wei, Zoltan Egyed, Victor Cotruta, Minh Giang, Phoebe Kirk, Anand Rao, Kat Black, Nabila Babar, Jessica Lo, Erica Moreira, Luiz Gustavo Martins, Omar Sanseviero, Lucas Gonzalez, Zach Gleicher, Tris Warkentin, Vahab Mirrokni, Evan Senter, Eli Collins, Joelle Barral, Zoubin Ghahramani, Raia Hadsell, Yossi Matias, D. Sculley, Slav Petrov, Noah Fiedel, Noam Shazeer, Oriol Vinyals, Jeff Dean, Demis Hassabis, Koray Kavukcuoglu, Clement Farabet, Elena Buchatskaya, Jean-Baptiste Alayrac, Rohan Anil, Dmitry Lepikhin, Sebastian Borgeaud, Olivier Bachem, Armand Joulin, Alek Andreev, Cassidy Hardin, Robert Dadashi, and Léonard Hussenot. Gemma 3 technical report, 2025. [5](#)

[17] Satoshi Tsutsui, Winnie Pang, and Bihang Wen. WBCAtt: A White Blood Cell Dataset Annotated with Detailed Morphological Attributes, 2023. arXiv:2306.13531 [cs]. [5](#)

[18] Zifeng Wang, Zhenbang Wu, Dinesh Agarwal, and Jimeng Sun. MedCLIP: Contrastive Learning from Unpaired Medical Images and Text, 2022. arXiv:2210.10163 [cs]. [2](#)

[19] Jason Wei, Xuezhi Wang, Dale Schuurmans, Maarten Bosma, Brian Ichter, Fei Xia, Ed Chi, Quoc Le, and Denny Zhou. Chain-of-Thought Prompting Elicits Reasoning in Large Language Models, 2023. arXiv:2201.11903 [cs]. [4](#)

[20] Chengrun Yang, Xuezhi Wang, Yifeng Lu, and Hanxiao Liu. LARGE LANGUAGE MODELS AS OPTIMIZERS. [2](#), [4](#), [7](#)

[21] Sheng Zhang, Yanbo Xu, Naoto Usuyama, Hanwen Xu, Jaspreet Bagga, Robert Tinn, Sam Preston, Rajesh Rao, Mu Wei, Naveen Valluri, Cliff Wong, Andrea Tupini, Yu Wang, Matt Mazzola, Swadheen Shukla, Lars Liden, Jianfeng Gao, Angela Crabtree, Brian Piening, Carlo Bifulco, Matthew P. Lungren, Tristan Naumann, Sheng Wang, and Hoifung Poon. BiomedCLIP: a multimodal biomedical foundation model pretrained from fifteen million scientific image-text pairs, 2025. arXiv:2303.00915 [cs]. [1](#), [2](#)

[22] Zihao Zhao, Yuxiao Liu, Han Wu, Mei Wang, Yonghao Li, Sheng Wang, Lin Teng, Disheng Liu, Zhiming Cui, Qian Wang, and Dinggang Shen. CLIP in Medical Imaging: A Comprehensive Survey, 2024. arXiv:2312.07353 [cs]. [2](#)

[23] Kaiyang Zhou, Jingkang Yang, Chen Change Loy, and Zizwei Liu. Conditional Prompt Learning for Vision-Language Models. In 2022 IEEE/CVF Conference on Computer Vision and Pattern Recognition (CVPR), pages 16795–16804, New Orleans, LA, USA, 2022. IEEE. [5](#)

[24] Kaiyang Zhou, Jingkang Yang, Chen Change Loy, and Zizwei Liu. Learning to Prompt for Vision-Language Models. International Journal of Computer Vision, 130(9):2337–2348, 2022. [1](#), [2](#), [5](#)

[25] Yongchao Zhou, Andrei Ioan Muresanu, Ziwen Han, Keiran Paster, Silviu Pitis, Harris Chan, and Jimmy Ba. Large Language Models Are Human-Level Prompt Engineers, 2023. arXiv:2211.01910 [cs]. [2](#)

Supplementary material

Meta-Prompts utilized for each dataset

This section presents the exact meta-prompts used for each dataset evaluated in this work.

Derm7pt [8] (Melanoma vs Non-melanoma binary classification)

- Q_0 — Initial meta-prompt

Listing 1. Initial meta-prompt for the Derm7pt dataset (Q_0).

```
Give 50 distinct textual descriptions of pairs of visual discriminative features to
identify whether a dermoscopic image of a skin lesion shows melanoma or not.
These are the following features an expert would look for: Pigment Network, Blue
Whitish Veil, Vascular Structures, Pigmentation, Streaks, Dots and Globules, Regression
Structures.
Each description pair must contain two contrasting features: one indicative of benign,
and one indicative of a melanoma

Only provide the output as Python code in the following format:
prompts = list[tuple[negative: str, positive: str]]
Let's think step-by-step
```

- Q_t — Mutation meta-prompt

Listing 2. Mutation meta-prompt for the Derm7pt dataset (Q_t).

```
The task is to generate distinct textual descriptions pairs of visual discriminative
features to identify whether a dermoscopic image of a skin lesion shows melanoma or not
.

These are the following features an expert would look for: Pigment Network, Blue
Whitish Veil, Vascular Structures, Pigmentation, Streaks, Dots and Globules, Regression
Structures.
Each description pair must contain two contrasting features: one indicative of benign,
and one indicative of a melanoma

Here are the best performing pairs in ascending order. High scores indicate higher
quality visual discriminative features.
Current top 10 prompt pairs:
1. ("....", "...."), Score: 60
2. ...
...

Write 10 new prompt pairs that are different from the old ones and has a score as high
as possible, formulate a strategy.
Only provide the output as Python code in the following format: prompts = list[tuple[
negative: str, positive: str]]. Let's think step-by-step
```

- Q_{crowd} — Crowding meta-prompt

Listing 3. Crowding meta-prompt for the Derm7pt dataset (Q_{crowd}).

```
The task is to group textual description pairs of visual discriminative features for
melanoma detection in a skin lesion.
Current Prompt Pairs: Format: <Index. Prompt Pair>
1. ("....", "....")
```

```
2. ...
3. ...
...
30. ...
```

Each pair corresponds to a feature of the same medical concept. Group the prompt pairs that has exactly same observation but differ only in language variations. Give the indexes of the grouped pairs in the output.
Provide the output as follows: list[list[index:int]]. Make sure to include all pairs in the output, even if they are not grouped with others.
Let's think step by step.

WBCAtt [17] (Peripheral Blood Smears: Multiclass Cell-type classification)

The following meta-prompts were utilized for the WBCAtt dataset, which focuses on multiclass cell-type classification in peripheral blood smears. For each one-vs-rest binary classifier, the variables `{BINARY_LABEL}` and `{other_labels_str}` are replaced with the specific cell-type being evaluated. The prompt leverages a set of defining attributes for each white blood cell type, which are stored in the `MEDICAL_CONCEPTS_MAPPING` dictionary. These attributes are:

- **Basophil:** Nucleus=Segmented, NC Ratio=Low, Granularity=Yes, Color=Blue/Black (dense)
- **Eosinophil:** Nucleus=Segmented, NC Ratio=Low, Granularity=Yes, Color=Red
- **Lymphocyte:** Nucleus=Unsegmented, NC Ratio=High, Granularity=No, Size=Small
- **Monocyte:** Nucleus=Unsegmented, NC Ratio=Low, Granularity=No
- **Neutrophil:** Nucleus=Segmented, NC Ratio=Low, Granularity=Yes, Color=Blue

- Q_0 — Initial meta-prompt

Listing 4. Initial meta-prompt for the WBCAtt dataset (Q_0).

```
Give 50 distinct textual descriptions of pairs of visual discriminative features to
identify whether the peripheral blood cell is a {BINARY_LABEL} or not. Other cell types
include {other_labels_str}.

These are the following features an expert would look for: Cell Size, Cell Shape,
Nucleus Shape, Nuclear-Cytoplasmic Ratio, Chromatin-Density, Cytoplasm-Vacuole,
Cytoplasm-Texture, Cytoplasm-Color, Granule-Type, Granule-Color, Granularity
{MEDICAL_CONCEPTS_MAPPING[BINARY_LABEL]}

Only provide the output as Python code in the following format: prompts = list[tuple[
negative: str, positive: str]]. Let's think step-by-step
```

- Q_t — Mutation meta-prompt

Listing 5. Mutation meta-prompt for the WBCAtt dataset (Q_t).

```
The task is to generate distinct textual descriptions of pairs of visual discriminative
features to identify whether the peripheral blood cell is a {BINARY_LABEL} or not.
Other cell types include {other_labels_str}.

These are the following features an expert would look for: Cell Size, Cell Shape,
Nucleus Shape, Nuclear-Cytoplasmic Ratio, Chromatin-Density, Cytoplasm-Vacuole,
Cytoplasm-Texture, Cytoplasm-Color, Granule-Type, Granule-Color, Granularity
{MEDICAL_CONCEPTS_MAPPING[BINARY_LABEL]}

Here are the best performing pairs in ascending order. High scores indicate higher
quality visual discriminative features.
```

```
Current top 10 prompt pairs:
1. ("....", "...."), Score: 60
2. ...
...
```

Write 10 new prompt pairs that are different to from the old ones and has a score as high as possible. Formulate a strategy",
Only provide the output as Python code in the following format: prompts = list[tuple[negative: str, positive: str]]. Let's think step-by-step

- Q_{crowd} — Crowding meta-prompt

Listing 6. Crowding meta-prompt for the WBCAtt dataset (Q_{crowd}).

The task is to group textual description pairs of visual discriminative features for white blood cell classification.

Current Prompt Pairs: Format: <Index. Prompt Pair>

```
1. ("....", "....")
2. ...
3. ...
...
30. ...
```

Each pair corresponds to a feature of the same medical concept. Group the prompt pairs that has exactly same observation but differ only in language variations. Give the indexes of the grouped pairs in the output.

Provide the output as follows: list[list[index:int]]. Make sure to include all pairs in the output, even if they are not grouped with others.

Let's think step by step.

Camelyon17-WILDS [9](Histopathology: Binary Classification)

- Q_0 — Initial meta-prompt

Listing 7. Initial meta-prompt for the Camelyon17-WILDS dataset (Q_0).

Give 50 distinct textual descriptions of pairs of visual discriminative features to identify whether the central region of a histopathological image patch contains tumor tissue or not. The patch is extracted from an H&E-stained whole-slide image of a lymph node section. Only provide the output as Python code in the following format: prompts = list[tuple[negative: str, positive: str]]

- Q_t — Mutation meta-prompt

Listing 8. Mutation meta-prompt for the Camelyon17-WILDS dataset (Q_t).

The task is to generate distinct textual descriptions pairs of visual discriminative features to identify whether the central region of a histopathological image patch contains tumor tissue or not. The patch is extracted from an H&E-stained whole-slide image of a lymph node section.

Here are the best performing pairs in ascending order. High scores indicate higher quality visual discriminative features.

Current top 10 prompt pairs:

```
1. ("....", "...."), Score: 60
2. ...
...
```

Write 10 new prompt pairs that are different to from the old ones and has a score as high as possible.

Only provide the output as Python code in the following format: prompts = list[tuple[negative: str, positive: str]]. Let's think step-by-step

- Q_{crowd} — Crowding meta-prompt

Listing 9. Crowding meta-prompt for the Camelyon17-WILDS dataset (Q_{crowd}).

The task is to group textual description pairs of visual discriminative features for tumor detection in histopathology.

Current Prompt Pairs: Format: <Index. Prompt Pair>

```
1. ("....", "....")
2. ...
3. ...
...
30. ...
```

Each pair corresponds to a feature of the same medical concept. Group the prompt pairs that has exactly same observation but differ only in language variations. Give the indexes of the grouped pairs in the output.

Provide the output as follows: list[list[index:int]]. Make sure to include all pairs in the output, even if they are not grouped with others. Let's think step by step

Sample LLM CoT Strategy

This section presents sample Chain-of-Thought (CoT) responses generated by the Gemma 3-27b-it LLM, demonstrating its reasoning process for our meta-prompts. Listing 10 and Listing 11 show two distinct examples of the strategy formulated by the LLM in response to the optimization meta-prompt (Q_t) for the Camelyon17-WILDS dataset. An example of the reasoning and final output for the crowding meta-prompt (Q_{crowd}) is provided in Listing 12.

Listing 10. Example of LLM's reasoning for the strategy as a response for the optimization meta prompt

Strategy to Enhance Prompt Fitness:

1. Highlight histopathological features that unambiguously separate benign/reactive from tumor tissue.
2. Use precise, quantifiable terms based on standard diagnostic criteria.
3. Introduce new descriptors-nuclear size & contour, chromatin texture, necrosis, apoptosis, cell cohesion, architectural disruption, cytoplasmic granularity, and hallmark patterns (e.g., starry sky, rosettes).
4. Craft negative prompts around the absence or benign manifestation of these features, and positive prompts around their abnormal or tumor-associated presentations.
5. Avoid repeating any feature pairs from the existing top-10 list.

Listing 11. Example of LLM's reasoning for the strategy as a response for the optimization meta prompt

Okay, let's break down a strategy to generate high-scoring prompt pairs for identifying tumor tissue in histopathological images.

1. Analyze Existing High-Scoring Pairs:

Specificity: The best pairs aren't just "normal" vs. "abnormal." They pinpoint specific features. "Abnormal cytoplasmic staining" is better than just "abnormal cells."

Visual Discriminability: The features must be readily observable in an H&E stain. Things like molecular markers are out of scope.

Tumor-Related Features: The features directly relate to hallmarks of cancer – abnormal growth, nuclear changes, necrosis, invasion, etc.

Contrast: The negative and positive prompts are clearly contrasting. "No mitotic figures" vs. "Frequent mitotic figures" is strong.

Lymph Node Context: Since the images are from lymph nodes, features related to lymph node architecture (lymphatic invasion, reactive follicles) are relevant.

2. Brainstorming Feature Categories:

Based on the above, let's consider categories of features to focus on:

Nuclear Features: Size, shape, chromatin, nucleoli, membrane irregularities. These are very important in cancer diagnosis.

Cytoplasmic Features: Staining intensity, granularity, presence of inclusions.

Growth Patterns: How cells are arranged (sheets, clusters, single cells, palisading).

Microenvironment: Inflammation, fibrosis, vascular changes, necrosis.

Invasion: Evidence of tumor cells breaking through boundaries (capsule, vessels, lymphatics).

Differentiation: Features suggesting the cell type or degree of differentiation (e.g., plasmacytoid differentiation).

3. Generating Prompt Pairs:

I'll aim for pairs that are:

Specific and visually discriminable.

Contrasting.

Relevant to lymph node pathology.

Different from the existing top 10.

Listing 12. Example of the LLM's reasoning and output in response to the crowding meta-prompt.

Let's think step by step. I will analyze the prompt pairs and group them based on identical observations with language variations.

- * Group 1: No plasma cells identified/observed/present
 - * 3: ('No plasma cells are identified.' , 'Numerous plasma cells with eccentric nuclei and abundant cytoplasm.')
 - * 12: ('No plasma cells are identified.' , 'Numerous plasma cells with eccentric nuclei are present.')
 - * 14: ('No plasma cells are observed.' , 'Increased number of plasma cells, some with Dutcher bodies.')
 - * 17: ('No plasma cells are identified.' , 'Increased number of plasma cells, some with Dutcher bodies.')
 - * 18: ('No plasma cells are present.' , 'Increased number of plasma cells with eccentric nuclei.')
 - * 22: ('No plasma cells are observed.' , 'Abundant plasma cells with eccentric nuclei.')
 - * 24: ('No plasma cells are identified.' , 'Abundant plasma cells with eccentric nuclei are present.')

* Group 2: Few reactive lymphocytes vs. Numerous reactive lymphocytes

- * 4: ('Few scattered reactive lymphocytes.' , 'Sheets of atypical lymphocytes with brisk proliferation.')
 - * 6: ('Few reactive lymphocytes are present.' , 'Dense infiltrate of atypical lymphocytes and plasma cells.')
 - * 8: ('Few reactive lymphocytes are present.' , 'Numerous reactive lymphocytes and plasma cells are observed.')
 - * 13: ('Few reactive lymphocytes present.' , 'Numerous reactive lymphocytes with plasmacytoid differentiation.')
 - * 25: ('Few reactive lymphocytes are present.' , 'Numerous reactive lymphocytes are present, forming rosettes around tumor cells.')
 - * 27: ('Few reactive lymphocytes.' , 'Abundant reactive lymphocytes and atypical lymphoid cells.')

- * 30: ('Few reactive lymphocytes present.' , 'Numerous reactive lymphocytes forming rosettes around tumor cells.')
- * Group 3: Lymphocyte maturity
 - * 9: ('Mature lymphocytes.' , 'Immunoblasts and plasmablasts.')
 - * 20: ('Lymphocytes are small and mature-appearing.' , 'Lymphocytes are large and immature-appearing with prominent nucleoli.')
 - * 29: ('Lymphocytes are small and mature.' , 'Lymphocytes are large and immature with prominent nucleoli.')
- * Group 4: Stroma cellularity
 - * 11: ('Stroma is edematous with minimal cellularity.' , 'Stroma is densely cellular with a myxoid appearance.')
 - * 28: ('Stroma is hypocellular with minimal collagen.' , 'Stroma is hypercellular with abundant collagen deposition.')
- * Group 5: Atypical plasma cells
 - * 19: ('No atypical plasma cells are identified.' , 'Presence of atypical plasma cells with prominent nucleoli.')
- * Group 6: Inflammatory infiltrate
 - * 15: ('Inflammatory infiltrate is minimal and lymphocytic.' , 'Dense inflammatory infiltrate with neutrophils and eosinophils.')
 - * 21: ('Minimal inflammatory infiltrate.' , 'Dense inflammatory infiltrate with numerous plasma cells.')
- * Group 7: Eosinophils
 - * 16: ('No eosinophils are present.' , 'Increased number of eosinophils infiltrating the tumor.')
- * Group 8: Emperipoleisis
 - * 10: ('No emperipoleisis is observed.' , 'Frequent emperipoleisis is seen within tumor cells.')
- * Group 9: Germinal Centers
 - * 26: ('Few reactive germinal centers.' , 'Numerous large and atypical germinal centers with prominent nucleoli.')
- * Group 10: Infiltration of atypical cells
 - * 1: ('No infiltration of atypical cells.' , 'Infiltration of atypical cells disrupting normal lymph node architecture.')
 - * 5: ('No infiltration of atypical cells into surrounding tissues.' , 'Infiltration of atypical cells into surrounding tissues, disrupting normal structures.')
- * Group 11: Cell Arrangement
 - * 2: ('Cells arranged in a normal lymphatic pattern.' , 'Cells arranged in sheets or solid nests.')
- * Group 12: Background Lymphoid Aggregates
 - * 23: ('Background shows normal lymphoid aggregates.' , 'Background shows diffuse sheets of atypical cells.')
- * Group 13: Immunocytes
 - * 7: ('Immunocytes are rare.' , 'Abundant immunocytes are present, forming rosettes.')

--- Final Output ---

[

```
[3, 12, 14, 17, 18, 22, 24],  
[4, 6, 8, 13, 25, 27, 30],  
[9, 20, 29],  
[11, 28],  
[19],  
[15, 21],  
[16],  
[10],  
[26],  
[1, 5],  
[2],  
[23],  
[7]  
]
```

Prompts Learnt

This section presents the final prompt ensembles (P^*) generated by BiomedXPro. We provide the prompts learned in two distinct experimental settings: the full-shot scenario, where the F1-macro score was used as the fitness metric, and the 1-shot scenario, where fitness was evaluated using the inverted Binary Cross-Entropy (BCE).

Derm7pt

The prompts learnt for the 1-shot and full-shot scenarios are listed in Tab. 3 and Tab. 4 respectively.

Table 3. Prompts Learned for the Derm7pt full dataset: F1-macro utilized as the fitness function

Absence or Normal Appearance (p_j^-)	Disease-Indicative Observations (p_j^+)	Fitness Score (s_j)
Pigmentation is limited to brown tones with sharp borders.	Pigmentation is variegated with shades of brown, black, blue, and grey, with ill-defined borders.	0.6741
Pigmentation is homogenous and limited to the epidermis.	Pigmentation is heterogeneous and extends into the dermis, causing a bluish hue.	0.6724
Blue-whitish veil is absent.	Blue-whitish veil is present and associated with ulceration.	0.6667
Pigmentation is limited to the periphery with a normal skin color center.	Pigmentation extends to the center of the lesion with shades of black, grey, and blue.	0.6565
Dots and globules have a smooth, rounded appearance.	Dots and globules are angular, irregular, and exhibit pseudopods.	0.6543
Pigmentation is light brown or tan.	Pigmentation is dark brown or black.	0.6535
Vascular structures show a regular, linear arrangement following skin creases.	Vascular structures display a chaotic, branching pattern with irregular vessel diameters.	0.6523
Vascular structures are primarily hairpin-shaped telangiectasias.	Vascular structures show branching vessels with irregular caliber and occasional hemorrhages.	0.6506
Pigmentation is predominantly brown with subtle variations.	Pigmentation includes shades of black, grey, and blue, with abrupt color changes.	0.6419
Vascular structures are primarily small, regularly spaced capillaries.	Vascular structures demonstrate large, dilated vessels and hemorrhages.	0.6392
The lesion exhibits a smooth, symmetrical surface with no evidence of ulceration or scarring.	The lesion exhibits an irregular, asymmetrical surface with ulceration, crusting, and surrounding inflammation.	0.635
Regression structures are absent or minimal, with slight lightening of the skin.	Regression structures are significant, with a scarred, fibrotic appearance and possible ulceration.	0.6324
The lesion exhibits a smooth, even surface texture.	The lesion demonstrates surface elevation, ulceration, or a nodular appearance.	0.6322
Streaks are fine and follow the natural skin creases.	Streaks are thick, irregular, and abruptly change direction, suggesting rapid growth.	0.6304

WBCAtt

The prompts learned for the **Neutrophil** class in the full-shot and 1-shot scenarios are shown in Tab. 5 and Tab. 6, respectively.

Camelyon17-WILDS

The prompts learned in both the 1-shot and 16-shot scenarios are shown in Tab. 7 and Tab. 8, respectively.

Table 4. Prompts Learned for the 1-Shot Derm7pt Case: Inverted BCE is utilized for the fitness function

Absence or Normal Appearance (p_j^-)	Disease-Indicative Observations (p_j^+)	Fitness Score (s_j)
Blue whitish veil is absent or minimal.	Blue whitish veil is pronounced and covers a significant portion of the lesion.	1.0
Blue whitish veil is absent or very subtle.	Blue whitish veil is prominent and widespread, obscuring the underlying structures.	1.0
Dots are evenly distributed and small.	Dots are clustered and large, with irregular shapes.	1.0
Dots and globules are small, round, and uniformly pigmented.	Dots and globules are large, irregular, and exhibit color variation.	1.0
Blue-whitish veil is absent or minimal, with no associated changes.	Blue-whitish veil is dense and associated with surrounding inflammation.	1.0

Table 5. Prompts Learned for Neutrophil Classification (Full-Shot Scenario): F1-macro as Fitness Function

Negative Class Observation (p_j^-)	Neutrophil-Indicative Observation (p_j^+)	Fitness Score (s_j)
The cell shape is consistently round with a smooth perimeter.	The cell shape is often irregular and slightly distorted due to the segmented nucleus.	0.7945
Cytoplasm is clear and homogenous, lacking distinct features.	Cytoplasm is abundant and contains fine, pale lilac granules.	0.7710
The nuclear shape is predominantly spherical with a smooth outline.	The nuclear shape is irregular and lobulated, with a clearly indented outline.	0.7565
Granules, if present, are sparse and difficult to discern.	Granules are abundant, easily visible, and fill a significant portion of the cytoplasm.	0.7487
The cell shape is generally round or slightly irregular.	The cell exhibits a more polymorphic shape, often displaying pseudopods or extensions.	0.7467
The cell shape is consistently oval or spherical, maintaining a regular form.	The cell shape is highly variable and often irregular, exhibiting pseudopod extensions.	0.7418
The cell shape is generally spherical or slightly irregular.	The cell exhibits an elongated or flattened shape.	0.7358
Granules, if present, are small and indistinct.	Granules are large, prominent, and easily identifiable.	0.7340
The cell size is similar to that of a small lymphocyte.	The cell size is significantly larger, comparable to a monocyte.	0.7242
The cell displays a uniform, homogenous cytoplasm without any noticeable texture.	The cell displays a granular cytoplasm with a slightly textured appearance.	0.7213
Granules, if present, are sparse and appear as small, indistinct dots.	Granules are numerous, prominent, and exhibit a distinct, segmented appearance.	0.7147
The cell exhibits a uniform, smooth cytoplasmic border.	The cell exhibits an irregular cytoplasmic border with occasional projections.	0.7133
The cell exhibits a high nuclear-cytoplasmic ratio, with the nucleus occupying most of the cell volume.	The cell displays a balanced nuclear-cytoplasmic ratio, with a substantial amount of cytoplasm.	0.7109
Granules, if present, are very few and evenly distributed.	Granules are numerous and clustered in specific areas of the cytoplasm.	0.7062

Table 6. Prompts Learned for Neutrophil Classification (1-Shot Scenario): Inverted BCE as Fitness Function

Negative Class Observation (p_j^-)	Neutrophil-Indicative Observation (p_j^+)	Fitness Score (s_j)
Basophils granules contain histamine and heparin, giving them a metachromatic staining property.	Neutrophils granules contain enzymes like myeloperoxidase and lysozyme, staining specifically with neutral dyes.	1.0000
Lymphocytes have a condensed, hyperchromatic nucleus.	Neutrophils have a segmented nucleus with varying degrees of chromatin condensation in each lobe.	1.0000
Basophils often have a U- or S-shaped nucleus due to the abundance of granules.	Neutrophils maintain a consistently segmented nuclear shape, even with granule presence.	1.0000
Eosinophils have granules that are rich in major basic protein and eosinophil cationic protein.	Neutrophils have granules containing elastase and collagenase.	1.0000
Basophils have granules that stain intensely with basic dyes.	Neutrophils have granules that stain weakly with both acidic and basic dyes.	1.0000
Basophils exhibit a high nuclear-cytoplasmic ratio, with a relatively small amount of cytoplasm.	Neutrophils have a low nuclear-cytoplasmic ratio, with a significant amount of cytoplasm.	0.9942
Lymphocytes have a consistently round nucleus.	Neutrophils have a segmented nucleus, typically with 3-5 lobes.	0.9515
Monocytes often present with a folded or irregular nuclear shape.	Neutrophils consistently display a segmented nucleus with distinct lobes.	0.5331
Basophils have intensely staining, dark purple granules that often fill the cytoplasm.	Neutrophils have granules that are less intensely stained and more evenly distributed within the cytoplasm.	0.2721
Eosinophils typically have a bilobed nucleus, although variations exist.	Neutrophils are characterized by a multi-lobed nucleus, usually with 3-5 lobes.	0.2497
Cells with a large, round nucleus and minimal cytoplasm are often lymphocytes.	Neutrophils are identified by their segmented nucleus and relatively large amount of cytoplasm.	0.2492
Eosinophilic cytoplasm is indicative of eosinophils.	The cytoplasm is pale blue or slightly pink.	0.2332
Monocytes typically exhibit a bean-shaped or kidney-shaped nucleus.	Neutrophils are defined by a multi-lobed, segmented nucleus.	0.2013

Table 7. Prompts Learned for Camelyon17-WILDS (1-Shot Scenario): Inverted BCE as Fitness Function

Absence or Normal Appearance (p_j^-)	Disease-Indicative Observations (p_j^+)	Fitness Score (s_j)
Cells arranged in a normal lymphatic pattern.	Cells arranged in sheets or solid nests.	0.9998
No infiltration of atypical cells.	Infiltration of atypical cells disrupting normal lymph node architecture.	0.9998
No plasma cells are identified.	Numerous plasma cells with eccentric nuclei and abundant cytoplasm.	0.9994
Few scattered reactive lymphocytes.	Sheets of atypical lymphocytes with brisk proliferation.	0.9992
Immunocytes are rare.	Abundant immunocytes are present, forming rosettes.	0.9988
Mature lymphocytes.	Immunoblasts and plasmablasts.	0.9987
No emperipoleisis is observed.	Frequent emperipoleisis is seen within tumor cells.	0.9986
Stroma is edematous with minimal cellularity.	Stroma is densely cellular with a myxoid appearance.	0.9984
No eosinophils are present.	Increased number of eosinophils infiltrating the tumor.	0.9980
Inflammatory infiltrate is minimal and lymphocytic.	Dense inflammatory infiltrate with neutrophils and eosinophils.	0.9980
No atypical plasma cells are identified.	Presence of atypical plasma cells with prominent nucleoli.	0.9979
Background shows normal lymphoid aggregates.	Background shows diffuse sheets of atypical cells.	0.9973
Few reactive germinal centers.	Numerous large and atypical germinal centers with prominent nucleoli.	0.9971
Lymphocytes show low proliferative activity.	Lymphocytes exhibit brisk proliferation with many dividing cells.	0.9966
Normal vasculature with thin walls.	Thickened and irregular vasculature with increased blood flow.	0.9962
Low nuclear-to-cytoplasmic ratio in lymphocytes.	High nuclear-to-cytoplasmic ratio in tumor cells.	0.9953
Germinal centers are small and inactive.	Germinal centers are large and hyperactive with numerous mitotic figures.	0.9947
Minimal inflammatory infiltrate.	Dense inflammatory infiltrate with lymphocytes and plasma cells.	0.9946
Adipose tissue is present in normal distribution.	Adipose tissue is compressed or replaced by tumor.	0.9946
Clear cytoplasm in lymphocytes.	Darkly stained, irregular cytoplasm in tumor cells.	0.9941
Lymphocytes are small and uniform.	Tumor cells are large and pleomorphic.	0.9941
No mitoses observed.	Frequent mitoses with atypical mitotic figures.	0.9940
Stroma is collagenous and hypocellular.	Stroma is fibrotic and hypercellular with increased mitotic activity.	0.9938
Few plasma cells are seen.	Numerous plasma cells with atypical morphology.	0.9937

Table 8. Prompts Learned for Camelyon17-WILDS (16-Shot Scenario): F1-macro as Fitness Function

Absence or Normal Appearance (p_j^-)	Disease-Indicative Observations (p_j^+)	Fitness Score (s_j)
No increase in mitotic activity.	Increased mitotic activity.	0.9193
No increase in eosinophilic cytoplasm.	Increased eosinophilic cytoplasm in tumor cells.	0.8982
Normal follicular architecture is preserved.	Disrupted follicular architecture with loss of polarity.	0.8904
Lymphocytes are small and round with dense nuclei.	Lymphocytes are large and atypical with prominent nucleoli.	0.8859
Benign inflammatory infiltrate.	Aggressive, atypical inflammatory infiltrate.	0.8837
No prominent nucleolus.	Large and prominent nucleoli within tumor cells.	0.8822
No increase in nuclear size.	Marked increase in nuclear size (nuclear pleomorphism).	0.8806
No atypical cells present.	Presence of atypical cells with pleomorphic nuclei.	0.8763
No fibrosis.	Increased stromal fibrosis surrounding tumor nests.	0.8748
No increase in interfollicular proliferation.	Increased interfollicular proliferation of atypical cells.	0.8663
No high-grade nuclear features.	Presence of high-grade nuclear features.	0.8627
Cells exhibit normal size and shape.	Cells exhibit significant variation in size and shape (anisocytosis and pleomorphism).	0.8532
No increased number of macrophages.	Increased number of macrophages infiltrating the tissue.	0.8490
Stroma with minimal collagen deposition.	Desmoplastic stroma with abundant collagen deposition.	0.8476
No spindle cell morphology.	Predominantly spindle cell morphology.	0.8298
No perivascular lymphocytic cuffing.	Perivascular lymphocytic cuffing around tumor nests.	0.8297
No increased nuclear-to-cytoplasmic ratio.	Increased nuclear-to-cytoplasmic ratio in tumor cells.	0.8278
No syncytial formation.	Syncytial formation of tumor cells.	0.8233
No evidence of extracellular mucin.	Presence of extracellular mucin surrounding tumor cells.	0.8225

Clinical Relevance Analysis

To provide a deeper, evidence-based validation of the prompts' clinical relevance, we ground our analysis in the statistical features of the training data. To create a quantitative measure of importance for the visual features in a dataset, we compute the conditional probability $P(\text{class} | \text{observation})$. This is calculated by dividing the number of images of a given class that exhibit a specific observation by the total number of images where that observation is present, across the training set. This probability serves as a data-driven proxy for the diagnostic significance of a visual feature.

Table 9. Conditional probabilities of melanoma given specific clinical observations, calculated on the Derm7pt training dataset (N=412).

Clinical Observation	P(Melanoma Obs.)
Vascular Structures: Linear Irregular	0.80
Blue-Whitish Veil: Present	0.59
Regression Structures: Combinations	0.58
Pigment Network: Atypical	0.55
Streaks: Irregular	0.53
Pigmentation: Diffuse Irregular	0.48
Vascular Structures: Dotted	0.48
Dots and Globules: Irregular	0.47
Regression Structures: White Areas	0.42
Pigmentation: Localized Irregular	0.33
Regression Structures: Blue Areas	0.33

Derm7pt Analysis

For the **Derm7pt** dataset, we calculated these probabilities for key dermatoscopic features associated with melanoma. The results are presented in Tab. 9. A detailed comparison between these statistical findings and the learned full-shot prompts (presented in Tab. 3) reveals a strong and consistent alignment:

- **Vascular Structures:** The most predictive feature, '*Linear Irregular*' *vascular structures* ($P = 0.80$), was captured by the high-fitness prompt pair (F1: 0.6523) that contrasts a '*regular, linear arrangement following skin creases*' with a '*chaotic, branching pattern with irregular vessel diameters*'.
- **Blue-Whitish Veil:** The second most significant feature, the presence of a '*Blue-Whitish Veil*' ($P = 0.59$), was identified by a high-scoring prompt (F1: 0.6667) distinguishing its absence from when it is '*present and associated with ulceration*'.
- **Regression Structures & Streaks:** Other key indicators like *regression structures* ($P = 0.58$) and *irregular streaks* ($P = 0.53$) were also identified, with prompts learning to contrast '*absent or minimal*' structures with '*significant, with a scarred, fibrotic appearance*,' and '*fine, natural*' streaks with those that are '*thick, irregular, and abruptly change direction*'.
- **Pigment Network:** Notably, while '*Atypical Pigment Network*' was a strong statistical indicator ($P = 0.55$), prompts describing nuanced aspects of pigmentation consistently achieved the highest F1-scores (up to 0.6741), such as the top-performing pair contrasting '*limited to brown tones with sharp borders*' with being '*variegated with shades of brown, black, blue, and grey*'.

WBCAtt Analysis

A similar analysis was performed for the WBCAtt dataset, focusing on the one-vs-rest classification of Neutrophils. We calculated the conditional probabilities for key cytological observations, presented in Tab. 10. The following is a detailed comparison between these statistics and the prompts learned in the full-shot scenario (presented in Tab. 5).

- **Granules:** The statistical data identifies the presence of '*Small*' and '*Pink*' granules as perfect predictors ($P = 1.00$). This is directly captured by the second-highest scoring prompt (F1: 0.7710), which contrasts a '*clear and homogenous*' cytoplasm with one that is '*abundant and contains fine, pale lilac granules*.' Multiple other high-fitness prompts also focus on the abundance and visibility of granules.
- **Nucleus Shape:** The '*Unsegmented-band*' nucleus shape is a highly significant statistical feature ($P = 0.85$). The framework learned this concept, generating a high-fitness prompt (F1: 0.7565) that distinguishes a '*predominantly spherical*' nucleus from one that is '*irregular and lobulated, with a clearly indented outline*'.
- **Complex Feature Learning:** Interestingly, while '*Irregular*' cell shape is a weak statistical predictor on its own ($P = 0.32$), the highest-scoring learned prompt (F1: 0.7945) is about cell shape. It learns a more complex, conditional feature

by contrasting a '*consistently round*' shape with one that is '*often irregular and slightly distorted due to the segmented nucleus*.' This shows the framework's ability to discover nuanced, multi-part features that are more discriminative than the simple statistical correlations.

This alignment demonstrates that BiomedXPro effectively identifies and articulates the key cytological features necessary for cell type classification.

Table 10. Conditional probabilities of a cell being a Neutrophil given specific cytological observations, calculated on the WBCAtt training dataset.

Cytological Observation	P(Neutrophil Obs.)
Granule Type: Small	1.00
Granule Colour: Pink	1.00
Nucleus Shape: Unsegmented-band	0.85
Granularity: Yes	0.43
Cytoplasm Colour: Light blue	0.43
Cytoplasm Texture: Clear	0.40
Nuclear-Cytoplasmic Ratio: Low	0.37
Cell Size: Big	0.36
Chromatin Density: Densely	0.35
Nucleus Shape: Segmented-multilobed	0.34
Cytoplasm Vacuole: No	0.34
Cell Shape: Round	0.32
Cell Shape: Irregular	0.32
Cell Size: Small	0.28
Nucleus Shape: Segmented-bilobed	0.20
Cytoplasm Vacuole: Yes	0.15

Limitation on Multiclass Classification

As mentioned in the main paper, while the one-vs-rest scheme is effective for extending our binary framework to multiclass problems, it can lead to the generation of over-specialized negative prompts (p_j^-). Instead of learning a general description for a "non-target" class, the evolutionary process often discovers that the most effective strategy is to describe a single, high-contrast competing class. The prompts learned for the **Eosinophil** class in the WBCAtt full-shot scenario provide a clear example of this behavior.

A review of the highest-scoring prompts (presented in Tab. 11) shows that the negative prompts are not general descriptions of blood cells, but are instead specific definitions of other cell types:

- The top-performing prompt (F1: 0.8311) uses a description of a **Neutrophil** for its negative case: '*Neutrophils exhibit granules that stain neutrally, appearing a faint lilac color.*'
- The second-highest scoring prompt (F1: 0.8247) uses a **Monocyte** as the negative exemplar: '*Monocytes exhibit a dull, greyish cytoplasm.*'
- The third-highest scoring prompt (F1: 0.8179) uses a **Basophil**: '*Basophils have granules that stain metachromatically, appearing purple-black.*'

This analysis shows that the framework effectively converts the one-vs-rest problem into a series of highly discriminative one-vs-one classifiers. While this is a powerful strategy for achieving high performance, it creates classifiers that may be brittle and less generalizable to the full spectrum of other classes. This finding further motivates the future work discussed in the main paper: extending the framework to natively handle a multiclass prompt set.

Table 11. Prompts Learned for Eosinophil Classification (Full-Shot Scenario)

Negative Class Observation (p_j^-)	Eosinophil-Indicative Observation (p_j^+)	Fitness Score (s_j)
Neutrophils exhibit granules that stain neutrally, appearing a faint lilac color.	Eosinophil granules are intensely stained with eosin, resulting in a bright red-orange color.	0.8311
Monocytes exhibit a dull, greyish cytoplasm.	Eosinophils display a cytoplasm with a pale pink or slightly orange hue.	0.8247
Basophils have granules that stain metachromatically, appearing purple-black.	Eosinophil granules stain specifically with eosin, resulting in a bright orange-red color.	0.8179
Basophils display dark blue or purple granules that often overwhelm the cytoplasm.	Eosinophil granules are characteristically bright pink or red-orange, contrasting with the basophilic granules of basophils.	0.8092
Monocytes display a folded or indented nuclear membrane.	Eosinophil nuclei are generally round or oval with a smooth, regular membrane.	0.8079
Monocytes exhibit a "cloud-like" or "ground glass" appearance to their cytoplasm.	Eosinophil cytoplasm is filled with distinct, refractile granules, lacking the diffuse appearance of monocytes.	0.8015
The cytoplasm of a lymphocyte is usually scant and clear.	Eosinophil cytoplasm is plentiful and filled with characteristic red-orange granules.	0.7971